J Solid State Electrochem (2010) 14:1325–1332
DOI 10.1007/s10008-009-0940-0

ORIGINAL PAPER

Controllable solvo-hydrothermal electrodeposition of lithium vanadate uniform carnation-like nanostructure and their electrochemical performance

Xueliang Li · Peipei Li · Mei Luo · Xiangying Chen · Jiejie Chen

Received: 28 July 2009 / Revised: 26 August 2009 / Accepted: 31 August 2009 / Published online: 1 October 2009

Abstract In this paper, we successfully developed a novel method to synthesize uniform carnation-like lithium vanadate nanostructures by combining electrochemical deposition and solvo-hydrothermal method. The samples were characterized by field emission scanning electron microscopy, power X-ray diffraction, and thermogravimetric analysis. The results show that the $LiV_3O_8 \cdot H_2O$ carnation-like nanostructure is 2–3 μm in diameter and assembled from nanosheets with thickness of 10–20 nm. Based on a series of experiments, we proposed a possible growth mechanism, in which the supersaturation derived from electric field and high conductivity under solvo-hydrothermal conditions due to the successive growth of lithium vanadate. In our work, we have discussed three different solvo-hydrothermal systems. It is proved that the morphology of coating materials could be conveniently controlled by selecting alcohols with different chain of alkyl. Compared with short-chain alcohol, $CH_3–(CH_2)_6–CH_2–OH$ was beneficial to promote the oriented growth of nanosheets. Electrochemical performances of lithium vanadate cathode materials were characterized by galvanostatic charge–discharge, and LiV_3O_8 synthesized in n-octanol aqueous solution exhibits the highest capacity of 357 mAh g^{-1} and best cycle stability. Furthermore, the influence of solvo-hydrothermal conditions on the morphology and electrochemical performance of products has also been studied.

X. Li (✉) · P. Li · M. Luo · X. Chen · J. Chen
Anhui Key Laboratory of Controllable Chemistry Reaction and Material Chemical Engineering, Hefei University of Technology, Hefei, Anhui 230009, China
e-mail: xueliangli2005@163.com

Keywords Solvo-hydrothermal · Electrochemical deposition · Lithium vanadate · Nanostructures · Electrochemical performance

Introduction

Controlled growth of nanostructures is of great importance in the field of nanoscience and nanotechnology and becomes a major concern in research areas such as materials science, electronics, and energy conversion [1, 2]. As an effective method to synthesize functional materials, electrochemical deposition plays an important role in forming multidimensional structure. The growth rate, the crystal size, and the surface morphology can easily be controlled by changing the electrodeposition parameters, such as deposition temperatures, potentials, current densities, and electrolyte composition. Recently, Li's group has made much work on preparing nanostructures by electrodeposition at room temperature. Bi/BiSb single crystalline nanowires [3] were electrodeposited, and they proposed corresponding growth mode. ZnO different nanostructures [4] were obtained by adjusting the current density. As positive materials, MnO_2 compounds [5] were synthesized by anodic oxidation of Mn^{2+} in hydrothermal solutions. The team of Yoshimura [6, 7] reported that ceramic and transition metal oxides films could be electrodeposited on some specifically metal substrates at room temperature or higher temperature. However, as far as we know, most of researches are limited to the formation of thin films. A general difficulty with film growth, the poor conductance of materials, became a barrier to continuous growth and ultimately resulted in self-limiting [8].

On the other hand, it is a fact that we are in such an epoch that various portable electronic devices are omni-

present in our daily life. Rechargeable lithium ion batteries seem to be a good choice since they can offer higher energy and power density, together with long-term cyclability. Among various candidates of lithium ion batteries cathode materials, lithium vanadium oxides have been extensively studied as positive materials due to high cell voltage, high specific capacity, and stability in air [9, 10]. It is well known that preparation methods have significant influence on the microstructure of materials and the electrochemical properties of lithium vanadium oxides [11]. The synthesis of LiV_3O_8 was carried out by reaction of Li_2CO_3 and V_2O_5 at 680°C for 10 h by traditional solid-state method [12]. This method usually produces sintered LiV_3O_8 with the low capacity of 180 mAh g^{-1} in the range of 1.8–4.0 V. Afterwards, many progresses have been made in improving preparation methods. The sol–gel route [13], hydrothermal method [14], microwave route [15], and spray-drying technique [16] were proposed to control the composition and homogeneity of products and decrease preparation time. Recently, more attention has been paid to enhance the specific capacity of lithium vanadium oxide materials [17–21]. The group of Guo did plenty of work on preparing lithium vanadium oxide composites, such as yttrium-doped LiV_3O_8 [19] and polypyrrole–LiV_3O_8 composite [20], which largely improved the electrical conductivity and stability of the composite electrode. And the fluorine content in fluorine-doped lithium trivanadates is proved to be affect the performance of LiV_3O_8 [21]. Meanwhile, it is interesting to note that some efforts have been paid on the preparation of LiV_3O_8 nanostructures to enhance electrochemical performance, such as nanorods [14], nanowires [22], and nanosheets [23]. Most recently, scientists studied the performance of LiV_3O_8 nanorods [24] in a wide voltage range of 1.5–4.5 V, and they got a high initial specific capacity of 348 mAh g^{-1} at the current density of 20 mA g^{-1}. Unfortunately, it was a long time approach with 114 h on the overall experiment. Still, it is believed that lithium vanadium oxide nanomaterials exhibit higher capacity and better cycle stability than bulk ones. Especially, flower-shaped nanoparticles may exhibit superior electronic performance than conventional materials [25]. In our previous work, we have paid great attention on fabricating electrode materials by hydrothermal route, such as orchid-like MnO_2 nanostructures [26] and VO_2 nanorods array [27]. Naturally, a novel method with easily control the morphology and crystalline orientation of electrode nanomaterials is highly desirable.

To date, fabrication of lithium vanadium oxides uniform nanostructures though solvo-hydrothermal electrochemical route is still a valuable challenge. In our work, peculiar carnation-like lithium vanadate nanostructures are firstly prepared by electrochemical approach. In the reaction system, solvent–hydrothermal technique and electrochemical method were sufficiently combined. Solvo-hydrothermal system may provide a good environment for electrochemical reaction, and the electric field can largely reduce the temperature and shorten reaction time. Considering the possible effect of organic solvent on electrodepositon, we chose alcohols with different chain of alkyl as additive and found their curial role in fabricating flower-like nanostructures. The electrochemical performance of lithium vanadate as cathode material in lithium ion batteries has also been studied.

Experimental

Sample preparation

Lithium vanadate nanostructures were prepared on CHI-660b electrochemical workstation using a three-electrotrode cell. The solvent–hydrothermal electrochemical system was set up with Tefion-lined stainless autoclave. Two titanium sheets were used as the working and the counter electrode, and Ag/Ag_2O electrode as the reference one. In a typical synthesis, 0.720 g V_2O_5 was mixtured with 50 ml LiOH (0.100 M). After V_2O_5 was reacted completely, 4.25 g LiCl was added as inert electrolyte. Then, the pH of the solution was adjusted to the range of seven to nine by adding appropriate LiOH. After solution changing to colorlessness, 40 mL n-octanol solution was added to the above solution. The mixture was vigorously stirred for 30 min at room temperature. We named this mixture as system A, in which the volume ratio of water and n-octanol was close to 1:1. Then, we prepared system B by adding 40 mL n-hexanol in the same way. By contrast, we also studied the system C by adding 40 mL deionized water instead of organic solvent.

The as-prepared solutions (system A, B, C) were transferred into a Teflon-lined three-electrode autoclave, and the autoclave connected to electrochemical workstation was sealed and maintained at 180°C for 3 h. Then, deposition was carried out at a constant potential of −1.2 V vs Ag/Ag_2O for 20–60 min. Meanwhile, the current was monitored as a function of time. After finishing deposition, the product was thoroughly rinsed with distilled water and dried for 3 h at 120°C. Before battery studies, the samples were annealed in air for 3 h at 450°C to remove the absorbed and crystal water in the products.

Sample characterizations

X-ray diffraction (XRD) pattern was recorded on a Japan Rigaku D/max-rB X-ray diffractometer with Cu Kα radiation (λ=1.5406 Å). Field emission scanning electron microscopy (FE-SEM) of the samples was performed on an FEI (Sirion200) scanning electron microanalyzer. Thermog-

ravimetric analysis (TGA) including TGA and differential thermal analysis (DTA) were carried out on a TGA-60 thermal analyzer (Shimadzu Corporation) with a heating rate of 10°C/min in flowing nitrogen.

The conductivity of dry lithium vanadate samples was measured by pressing a small amount of dry products to be a wafer, with area of 6.86×10^{-3}cm^2 and the thickness of 0.01 cm, and measuring the through-plane resistance R with a multimeter. The specific conductivity was calculated from the thickness d of the wafer and its radius r according to $\sigma=d/(R\pi r^2)$. For a given sample, conductivity values under different temperature were also obtained.

Electrochemical charge–discharge cycle performance of the samples was evaluated in model CR2032 coin cells. The composite cathode consisted of active LiV_3O_8 materials, acetylene black, and polyvinylidene difluoride at a weight ratio of 80:15:5. The mixture was coated onto an aluminum foil, pressed into a disk, and then dried under vacuum at 100°C for 16 h. This disk and a foil of lithium metal were used as the positive and negative electrodes, respectively. The electrolyte was 1 M $LiPF_6$ in 1:1 ethylene carbonate and diethyl carbonate electrolytes, and the separator was Celgard 2400 microporous polypropylene membrane. The cells were assembled in a dry glove box filled with highly pure argon gas (O_2 and H_2O levels <1 ppm). The galvanostatic charge–discharge test was conducted by a BTS-55 Netware battery testing system at a current of C/10 in the voltage range 2.0–4.0 V versus Li/Li^+. For calculating the C rate of charge–discharge, a theoretical capacity of 372 mAh g^{-1} of LiV_3O_8 was assumed. All the tests were performed at 25°C.

Results and discussion

Morphology and structure

XRD analyses The XRD patterns of lithium vanadate calcined at various temperatures (120, 250, 350, and 450°C) for 3 h were presented. As shown in Fig. 1, with the increase of annealing temperature, the intensity of diffraction peaks becomes stronger, which indicates that there is an obvious difference among the structure of four samples. In Fig. 1a, b, there is no obvious diffraction peaks and the LiV_3O_8 phase cannot be observed. The original products exhibit the characteristic of the amorphous substance. Then, the lithium vanadate compounds with monoclinic crystal structure appear at the calcined temperature of 350°C (Fig. 1c). Almost all of the peaks can be indexed to the LiV_3O_8 structure (JCPDS card No: 72-1193), and they are assigned to (100), (002), (003), $(\bar{1}11)$, (103), $(\bar{3}01)$, and (020) planes of LiV_3O_8, respectively. But the diffraction intensities are still weak, and this

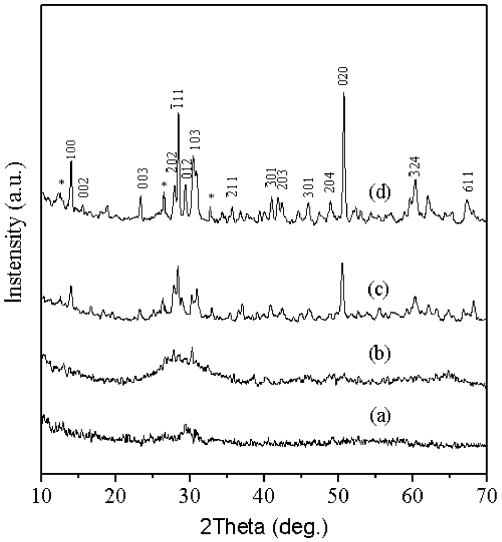

Fig. 1 XRD patterns of the samples calcined at different temperatures: 120 (*a*), 250 (*b*), 350 (*c*), and 450°C (*d*). $Li_{0.3}V_2O_5$ (*asterisk*)

means that the LiV_3O_8 phase is still not totally formed. The X-ray diffraction pattern of Fig. 1d shows that diffraction peaks become sharper and higher after annealing at 450°C. Meanwhile, there are few weak peaks of $Li_{0.3}V_2O_5$ (JCPDS card No: 18-0755) appearing at $2\theta=12.29$, 26.48, 32.72 (marked by asterisk). But the intensity of peak is relatively weak comparing with that of the LiV_3O_8, indicating that the monoclinic phase of LiV_3O_8 is the dominant phase. Owing to the diversity of lithium vanadium oxide compounds, it was possible that partial V^{5+} in LiV_3O_8 was deoxidized to lower valences on the cathode working electrode while deposition. By the way, this impurity phase of $Li_{0.3}V_2O_5$ was also reported to be existed with LiV_3O_8 materials in other works [15, 21, 22].

From the analysis above, we learned that lithium vanadate materials prepared by electrochemical method exhibit poor crystalline, unlike that prepared by conventional long-time high temperature synthesis. Compared with traditional method, the electrodeposition runs too fast to have little chance of forming ordered phases. The small crystallites and poor crystallinity gave rise to the broad and weak diffraction peak at lower drying temperatures in XRD patterns. From XRD analysis, we also conclude that samples produced become LiV_3O_8 crystals from amorphous during annealing treatment.

Thermal analyses The TGA/DTA plot (Fig. 2) recorded in flowing nitrogen from 36 to 600°C. The weight change profile for the coating material exhibits a steep loss between 36 and 140°C, followed by a gradual weight loss until 400°C. From 400 to 600°C, the sample weight remained constant.

The TGA plot shown in Fig. 2 exhibits a weight loss up to 600°C, which is related to the procedure of dehydration.

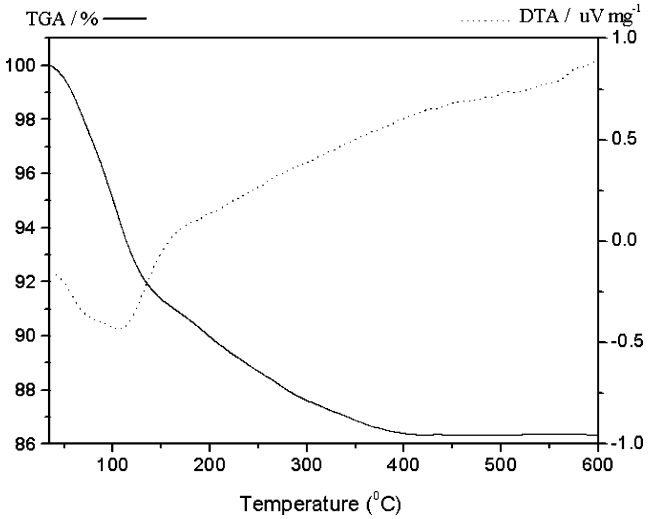

Fig. 2 TGA/DTA curves of original product deposited at the solvo-hydrothermal temperature of 180 °C

A weight loss of 8.29% below 140 °C may be due to the release of water absorbed on the sample's surface. In the temperature range of 140–400 °C, it exhibits a weight loss of 5.81% that may be attributed to the release of water in the crystal. Assuming the phase of product after deposition is $LiV_3O_8{\cdot}H_2O$, the theoretical weight percentage content of the water in crystal is 5.89%. This is close to that obtained from the TGA analysis, and the error maybe due to the little existence of impurity $Li_{0.3}V_2O_5$. Correspondingly, DTA curve exhibits an increasing trend after 200 °C, which could be attributed to the continuous crystallization of LiV_3O_8 phase.

The analysis from TGA/DTA proves the transform of amorphous to crystalline of products. As pointed in XRD patterns, the sample calcined at 120 °C did not present any diffraction peak which ascribed to amorphous LiV_3O_8. The X-ray diffraction peaks become obvious and sharp at 450 °C, and the LiV_3O_8 phase is totally formed. As we can conclude, the coating materials grown in this approach are amorphous and should be annealed to crystallize into the LiV_3O_8 phase.

SEM pictures The FE-SEM pictures of products deposited in different systems are shown in Figs. 3 and 4. For the lithium vanadate nanostructures prepared at mild temperature of 180 °C, a systematic research on morphology and structure of products via n-octanol aqueous solution (system A), n-hexanol aqueous solution (system B), and aqueous solution (system C) are presented.

As shown in the general image of Fig. 3a, b, large area lithium vanadate carnation-like arrays were obtained in system C (without organic solvent).The peculiar structures look like lots of carnations consisting of petals connected with each other. The petals appear to have sharp edges, with the average thickness of 10–20 nm and the diameter of

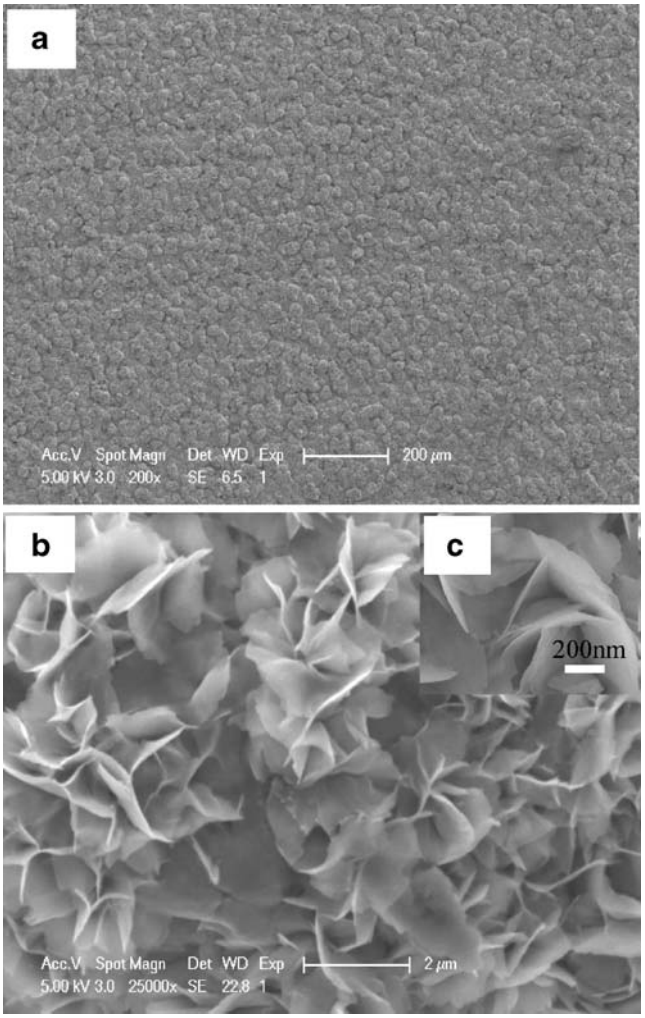

Fig. 3 SEM images of large-area carnation-like LiV_3O_8 deposited under a current density of 6 mA cm^{-2} at 180 °C: ×200 (**a**), ×25,000 (**b**), and its partial magnification inserted (**c**)

1–2 μm from the insert magnified SEM image (Fig. 3c). These petal-like structures appear to randomly distribute along different directions on the substrate.

In order to investigate the role of solvents, the high magnification SEM images in Fig. 4 present morphologies of samples synthesized in systems A, B, and C. Seem from Fig. 4, obvious changes can be observed. In image Fig 4a, the significant petal-like bending can be found, and petals randomly grow along different directions. In image Fig. 4b, nanosheets become more vertically grown on the substrate and appear to largely improve the alignment and vertical direction, although there was still slight bending. In contrast, in image Fig. 4c, nanosheets (with similar thickness of 10–20 nm) become substantially straight and parallel to assemble nanowall structures. These nanowall structures not only are perpendicular to the substrate, but also form groups of parallel nanowalls closely aligned in one direction.

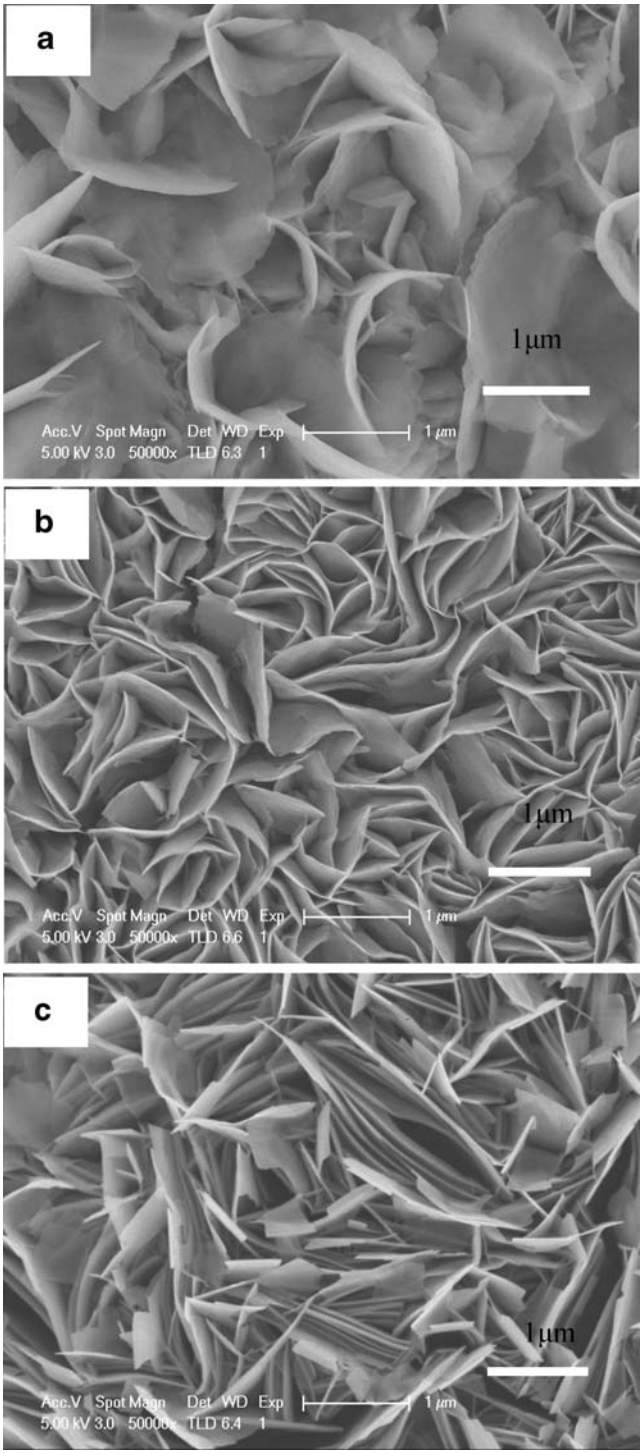

Fig. 4 SEM images of products deposited in different solvo-hydrothermal systems. **a** Aqueous solution. **b** n-Hexanol solution. **c** n-Octanol aqueous solution

Obviously, the crystal configurations and the distribution of crystal size were affected by the solvent. It promotes the transform of particles structure, including the change from randomly oriented and poorly crystalline nanosheets to well-aligned nanowalls. It suggests that the particle shape of $LiV_3O_8{\cdot}H_2O$ is related to the makeup of alcohols, especially, long-chain alcohol favors to the preferential ordering of crystals. We suppose that alcohols absorbed on the cathode surface play effective role as soft template.

Therefore, it is concluded that both the deposition and the crystal growth of lithium vanadate strongly depend on electrolyte composition, namely the morphology of the deposited lithium vanadate can be conveniently controlled by varying organic solvents.

Growth processes and reactions

In our study, large-scale lithium vanadate 2D nanosheets were successfully deposited by solvo-hydrothermal electrochemical approach at 180 °C. It was found that all products directly deposited on the cathode.

We proposed a possible growth mechanism as follows: The potential at −1.2 V vs Ag/Ag_2O is loaded onto the working electrode. Meanwhile, H^+ and Li^+ ions are moving forward to the working electrode because of the negative potential. The concentration of Li^+ rapidly increases around cathode due to its congregated. There are several combinations between cations (H^+, Li^+) and anions (OH^-, Cl^-, VO_3^-) in the electrolytic solution, while the solubility of the compound consisting of Li^+ and VO_3^- is quite low among them. Thus, the increase in the amount of Li^+ ions leads to deposition of the supersaturated lithium vanadate. Therefore, it seems that the supersaturation derived from electric field play a key role in the cathode deposition of lithium vanadate.

In our synthesis system, the predominant ions of the electrolytic solution used are Li^+ and Cl^-. Thus, during the loading of cathode potential, the electric charge was mainly used for the reduction of H_2O to H_2 gas at the cathode and oxidation of Cl^- to Cl_2 gas at the anode. The main electrode reactions at cathode and anode can be introduced as follows:

$$Li^+ + 3VO_3^- + 4H_2O + 2e \rightarrow LiV_3O_8 \cdot H_2O + 4OH^- + H_2 \uparrow$$

$$\mathbf{2}Cl^- \rightarrow Cl_2 \uparrow + 2e$$

And the small amount of $Li_{0.3}V_2O_5$ deposited on cathode electrode maybe induced by the reaction: $0.3Li^+ + 2VO_3^- + H_2O + 0.3e \rightarrow Li_{0.3}V_2O_5 + 2OH^-$

In the present study, the pH value of the solution increased after the experiment. This phenomenon is consistent with the reactions. Meanwhile, so as to maintain successive electrochemical growth, it is important for film to have good conductivity. As we know, the good conductivity can be achieved by rising hydrothermal temperature.

The discussion above indicates that the local supersaturation on the working electrode interface and hydrothermal condition mainly determine the growth of $LiV_3O_8{\cdot}H_2O$.

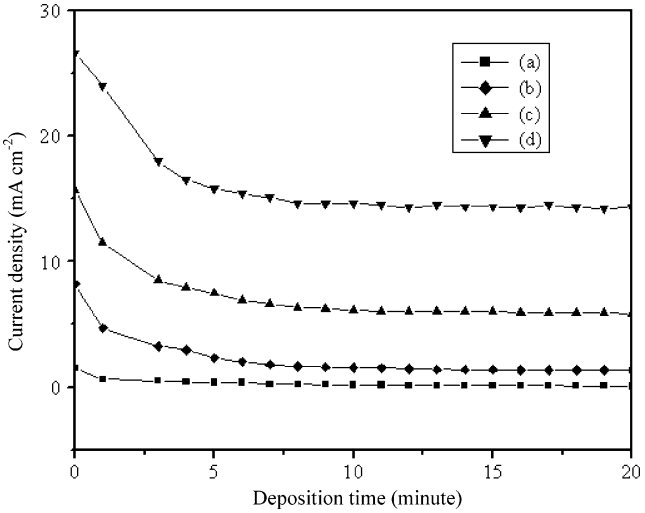

Fig. 5 Plots of current density vs deposition time under different solvo-hydrothermal temperatures: 100 (*a*), 140 (*b*), 180 (*c*), and 220 °C (*d*)

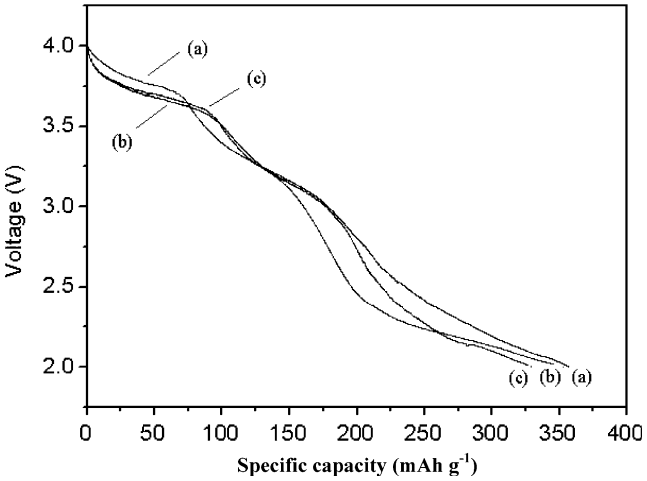

Fig. 7 The first discharge curves of LiV_3O_8 synthesized in different systems: n-octanol aqueous solution (*a*), n-hexanol aqueous solution (*b*), and aqueous solution (*c*)

Furthermore, some results in our work can support the growth mechanism. Seen from Fig. 5, the current was found rapidly increasing with deposition temperature. In every curve, the current become very stable after the beginning of drop. Along with the successive current, the deposition process was conducted. However, the current density rapidly decreased close to zero at the hydrothermal temperature of 100 °C, and only thin film has been found on the substrate. We assumed that the thin film with poor conductivity prevented the successive reactions. The materials for continuous electrodeposition ought to have reasonable electrical conductivity at the operating temperatures. Therefore, a higher temperature was needed in order to raise the conductivity of lithium vanadate materials, then the successive growth of the $LiV_3O_8{\cdot}H_2O$ crystal could be achieved. Owing to the good crystallization and high conductivity under hydrothermal conditions, we choose the deposition temperature of 180 °C. A mass of products quickly synthesized under the current density of 6 mA cm^{-2}. Actually, the appearance of sustaining current indicated that the deposited lithium vanadate materials were conductive enough, which promoted electron transfer to the substrates.

Figure 6 shows that the conductivity of products is dramatically affected by temperature. The calculated specific conductivity σ_0 at 20 °C is 3.54×10^{-4} S cm^{-1}, which is approaching to literatures reported [15, 16]. And the relative conductivity σ/σ_0 in function of temperature was given in Fig. 6 with partial enlarged drawing. Evidently, the

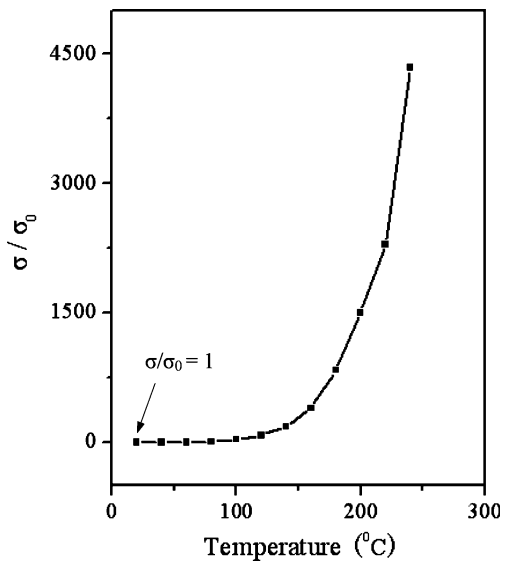

Fig. 6 Variable–temperature conductivity of dry product prepared at the current density of 6 mA cm^{-2}

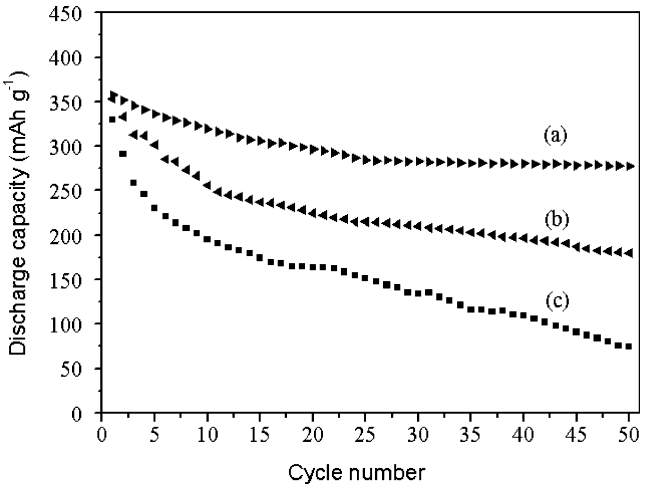

Fig. 8 Discharge cycling capacity of samples synthesized in different systems: n-octanol aqueous solution (*a*), n-hexanol aqueous solution (*b*), and aqueous solution (*c*)

curve exhibits a sharp increase at 180 °C. This result is in great agreement with information from Fig 5. When hydrothermal temperature was higher than 180 °C, the current density exhibited a rapid increase. The excellent conducting layer promotes the continuous current density of 6 mA cm^{-2}. Therefore, the continuous current density is related to high conductivity of products. These discussion explained the rationality of growth mechanism of $LiV_3O_8 \cdot H_2O$ as we proposed.

Electrochemical properties

The initial discharge curves of cells from LiV_3O_8 that prepared in systems A, B, and C are illustrated in Fig. 7a–c, respectively. In the voltage range of 2.0–4.0 V, the discharge specific capacity of sample A is 357 mAh g^{-1}, which is higher than that of sample B (353 mAh g^{-1}) and sample C (329 mAh g^{-1}). The high capacity of 357 mAh g^{-1} is close to the theoretical capacity of 372 mAh g^{-1}. We maintained that the high capacity may be not only because of the formation of uniform nanostructures by the novel method, but also due to the smaller particle size realized by the low temperature of annealing. And the good conductivity of lithium vanadium oxide materials also made a crucial effect on the good performance.

The cycling behaviors of as-prepared LiV_3O_8 nanomaterials (samples A, B, and C) were investigated at a current of 1/10C between 4.0 and 2.0 V vs Li/Li^+. Figure 8 displays the specific discharge capacities as a function of the cycle number. It can be seen that the samples synthesized via this novel method exhibit good capacity retention in 50 cycles. As can been seen, in the beginning 25 cycles, the discharge capacity of samples synthesized in systems A, B, and C are 284, 215, and 151 mAh g^{-1}, respectively. Among the next 25 cycles, sample C both show rapid capacity fading, and sample B presents better stability than C, which may be due to the compact nanostructures. However, it is interesting that sample A with nanowalls structures exhibits little capacity fading from 25 to 50 cycles; with the specific capacity of 277 mAh g^{-1} after 50 cycles, sample A retains as high as 97% of its capacity from 284 mAh g^{-1} at 25 cycles. In the voltage range of 2.0–4.0 V, this result is much better than the references reported [23, 24]. The material displays good capacity retention at the current of 1/10C.

Furthermore, as we found the good cycling ability of sample A, it is necessary for us to study more about the material. In a typical experiment with sample A, we broadened the voltage range to 1.8–4.0 V after 50 cycles. It was amazing that the capacity ascended to 308 mAh g^{-1}, and it cycled for five cycles with almost no fading.

It can be seen that samples prepared in n-octanol solution exhibit the best cycling capability, which indicates that the nanowalls with superposition structure are stable during the process of charge–discharge. From the discussion above, we can see that the morphology of samples can be controlled by varying solvents, and the samples electrodeposited in long chain alcohols aqueous solution demonstrated better electrochemical properties.

Conclusions

Lithium vanadate nanostructures with flower-like nanosheets and nanowalls morphology were successfully deposited by solvo-hydrothermal electrochemical route. Owing to introducing electrodeposition, lithium vanadate materials can be rapidly synthesized at a relatively lower temperature of 180 °C. Due to the supersaturation of lithium vanadate derived from electric field, large-scale flower-like nanostructures were deposited on the cathode electrode, and the petal-like nanosheets with the thickness of 10–20 nm were seen from FE-SEM. The successive growth of products have benefited from the good conductance of lithium vanadate at 180 °C. Organic solvents were found to play a significant role in controlling the morphology of nanostructures. Specially, alcohols with long chain have promoted the oriented growth of nanosheets as soft template. Hereby, a possible mechanism was proposed for explaining the electrochemical growth of $LiV_3O_8 \cdot H_2O$.

The products presented good electrochemical performance as cathode materials in lithium ions batteries. Compared with samples prepared in other solvents, LiV_3O_8 deposited in n-octanol aqueous solution exhibited higher discharge capacity of 357 mAh g^{-1} and better cycle capability. The good performances maybe result from the stability of aligned nanowalls in charging−discharging processes. Furthermore, this rapid and controllable route may extend to synthesize other transition metal oxides with multidimensional morphologies.

Acknowledgment This work was financially supported by the annual key project of Anhui Province of China (no. 07020203003 and no. 08020203005)

References

1. Fuhrer MS, Nygard J, Shih L, Forero M, Yoon YG, Mazzoni MSC, Choi HJ, Ihm J, Louie SG, Zettl A, McEuen PL (2000) Science 288:494
2. Hu J, Odom TW, Lieber CM (1999) Acc Chem Res 32:435
3. Xincun D, Guanghai L, Hechang L (2008) Nano Letters 8(5):1286–1290
4. Bingqiang C, Xuemei T, Sung Hwan H, Yue L, Sung Oh C, Guanghai L, Weiping C (2007) J Phys Chem C 111:2470
5. Hill LI, Verbaere A, Guyomard D (2003) J Power Sources 119:226
6. Yoshimura M, Suchanek WL, Byrappa K (2000) MRS Bull 25:17

7. Lee JH, Han KS, Lee BJ, Seo SI, Yoshimura M (2004) Electrochim Acta 50:467
8. Jayakrishnan R, Hodes G (2003) Thin Solid Films 440:19
9. Pistoia G, Panero S, Tocci M, Moshtev RV, Manev V (1984) Solid State Ionics 13:311
10. Manev V, Momchilov A, Nassalevska A, Pistoia G, Pasquali M (1995) J Power Sources 54:501
11. Murphy DW, Christian PA, Disalvo FJ, Carides JN (1979) J Electrochem Soc 126:497
12. Wadsley AD (1957) Acta Cryst 10:261
13. Dubarry M, Gaubicher J, Guyomard D, Durupthy O, Steunou N, Livage J, Dupre N, Grey CP (2005) Chem Mater 17:2276
14. Xu HY, Wang H, Song ZQ, Wang YW, Yan H, Yoshimura M (2004) Electrochim Acta 49:349
15. Yang G, Wang G, Hou WH (2005) J Phys Chem B 109:11186
16. Tran N, Bramnik KG, Hibst H, Prolss J, Mronga N, Holzapfel M, Scheifele W, Novak P (2008) J Electrochem Soc 155:A384
17. Gao H, Jiang CY, Wan CR (2004) J Power Sources 125:90
18. Jiao LF, Liu L, Sun JL, Yang L, Zhang YH, Yuan HT, Wang YM, Zhou XD (2008) J Phys Chem C 112:18249
19. Feng CQ, Huang LF, Guo ZP, Wang JZ, Liu HK (2007) J Power Sources 174:548
20. Chew SY, Feng CQ, Ng SH, Wang JZ, Guo ZP, Liu HK (2007) J Electrochem Soc 154:A633
21. Liu YM, Zhou XC, Guo YL (2009) Electrochim Acta 54:3184
22. Liu XH, Wang JQ, Zhang JY, Yang SR (2007) J Mater Sci 42:867
23. Gu YX, Chen DR, Jiao XL, Liu FF (2006) J Mater Chem 16:4361
24. Liu HM, Wang YG, Wang KX, Wang YR, Zhou HS (2009) J Power Sources 192:668
25. Zhang H, Cao GP, Wang ZY, Yang YS, Shi ZJ, Gu ZN (2008) Nano Letters 8:2664
26. Li XL, Li WJ, Chen XY, Shi CW (2006) J Cryst Growth 297:387
27. Li XL, Chen XJ, Chen XY, Han CL, Shi CW (2007) J Cryst Growth 309:43